ACS APPLIED MATERIALS & INTERFACES

Research Article

www.acsami.org

Lead-Free Piezoceramics: Revealing the Role of the Rhombohedral–Tetragonal Phase Coexistence in Enhancement of the Piezoelectric Properties

Fernando Rubio-Marcos,[*,†,∥] Rigoberto López-Juárez,[*,‡,∥] Rocio E. Rojas-Hernandez,[†] Adolfo del Campo,[†] Neftalí Razo-Pérez,[§] and Jose F. Fernandez[†]

[†]Electroceramic Department, Instituto de Cerámica y Vidrio, CSIC, Kelsen 5, 28049 Madrid, Spain

[‡]Unidad Morelia del Instituto de Investigaciones en Materiales, Unidad Morelia, and [§]Escuela Nacional de Estudios Superiores, Universidad Nacional Autónoma de México, Antigua Carretera a Pátzcuaro No. 8701, Col. Ex Hacienda de San José de la Huerta, C.P. 58190, Morelia, Michoacán, México

Supporting Information

ABSTRACT: Until now, lead zirconate titanate (PZT) based ceramics are the most widely used in piezoelectric devices. However, the use of lead is being avoided due to its toxicity and environmental risks. Indeed, the attention in piezoelectric devices has been moved to lead-free ceramics, especially on $(K,Na)NbO_3$-based materials, due to growing environmental concerns. Here we report a systematic evaluation of the effects of the compositional modifications induced by replacement of the B-sites with Sb^{5+} ions in $0.96[(K_{0.48}Na_{0.52})_{0.95}Li_{0.05}Nb_{1-x}Sb_xO_3]$-$0.04[BaZrO_3]$ lead-free piezoceramics. We show that this compositional design is the driving force for the development of the high piezoelectric properties. So, we find that this phenomenon can be explained by the stabilization of a Rhombohedral–Tetragonal ($R-T$) phase boundary close to room temperature, that facilities the polarization process of the system and exhibits a significantly high piezoelectric response with a d_{33} value as high as ~400 pC/N, which is comparable to part soft PZTs. As a result, we believe that the general strategy and design principles described in this study open the possibility of obtaining $(K,Na)NbO_3$-based lead-free ceramics with enhanced properties, expanding their application range.

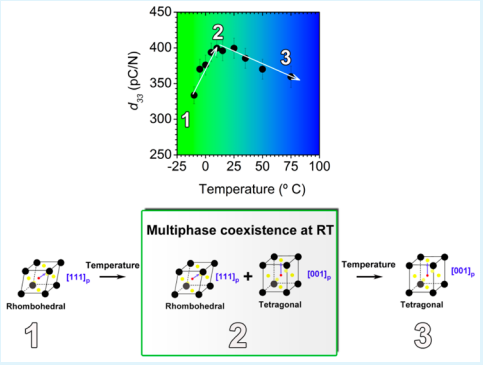

KEYWORDS: *lead-free piezoceramics, ferroelectric, piezoelectric, niobates, multiphase coexistence*

1. INTRODUCTION

Lead zirconate titanate (PZT) based ceramics are the most widely used piezoelectric until now, because of their high piezoelectric response, large scale production capability, and the possibility of tailoring their properties through composition.[1] The European Union has published a health normative (Restriction of Hazardous Substances, RoHS)[2] avoiding the use of lead due to its toxicity and environmental risks. Nevertheless, PZT ceramics are temporarily tolerated because of the lack of an adequate alternative.

Over the past few years, attention has been moved to lead-free ceramics,[3−9] in particular, to potassium–sodium niobate (KNN)-based materials. KNN is a good candidate for the replacement of lead zirconate-titanate,[8−12] but its properties need to be increased in order to reach the PZT ones. Recent efforts for enhancing the properties in KNN ceramics have been concentrated on chemical optimization through doping,[5,8−15] controlling the sintering process,[2,3] and domain engineering by adjusting the poling stage.[11,15,16] However, implementations of modified KNN ceramics for commercial use are still limited by their inferior electrical and electromechanical properties as compared to their conventional PZT counterparts. Exceptionally high piezoelectric properties were reported in the $(K,Na)NbO_3$–$LiTaO_3$–$LiSbO_3$ (KNL-NTS hereafter), a system proposed by Saito et al. in 2004.[10] This study was based on chemical modifications, in the vicinity of the morphotropic phase boundary, MPB, of $(K,Na)NbO_3$ (KNN), by complex simultaneous substitutions in the A (Li) and B (Ta and Sb) sites of the perovskite structure. Besides these chemical modifications, materials were developed following a novel processing route for producing textured polycrystals of the KNN-based compositions by additional engineering of the microstructural design. However, the compositional inhomogeneity, particularly the inhomogeneous distribution of Nb^{5+}, Ta^{5+}, and Sb^{5+} on the B-site of the perovskite structure, is rather difficult to avoid due to the phase segregation of end members over a wide temperature interval.[17] In addition, apparent compositional segregation in KNN has been evidenced in ceramics annealed for a long time.[18] More recently, new material systems based on KNN ceramics have

Received: July 24, 2015
Accepted: October 5, 2015
Published: October 5, 2015

DOI: 10.1021/acsami.5b06747
ACS Appl. Mater. Interfaces 2015, 7, 23080−23088

been designed and developed for obtaining a new phase boundary and a large d_{33}.[19−24] Those ceramics possess high d_{33} performance, which was obtained by designing and optimization of a Rhombohedral−Tetragonal ($R-T$) phase boundary. So, these results have opened up a challenge to obtain lead-free piezoceramics with good properties without the need of special processing. At the present time, these compounds could be considered as candidates for the substitution of PZT.[19−24] Although this rapid progress suggests that even higher piezoelectric properties are at hand for the KNN-based system, the confirmation of basic piezoelectricity credentials increases the importance of other issues in determining the technology's ultimate fate. Nevertheless, some of their properties and compositional features, such as the Ta^{5+} presence, are not suitable for all issues because tantalum oxide, Ta_2O_5, is scarce and expensive. Thus, the addition of Ta^{5+} should be avoided as far as possible or be used with a low content in terms of their practical applications.

We have reported in the KNN-based system, that the dielectric, piezoelectric, and elastic material responses are fundamentally related to extrinsic effects.[25] Nonetheless, the dielectric and mechanical losses at room temperature are similar to those of a soft PZT ceramic and are too high to be used in power devices. Thus, these materials need to be modified by the use of suitable dopants, like for "pure" KNN. The effect of doping on various physical and chemical properties of this material is considered as a classic story in the field of piezoelectric materials, which are used to modify the crystal structure and the piezoelectricity of these systems. Many aliovalent compositional modifications to the KNN-based system have been studied either with higher valence substitutions (donors) or with lower valence ions (acceptors). Doping KNN promotes formation of a polymorphic phase transition (*PPT*) in Li^+, Sb^{5+}, and Ta^{5+} doped KNN ceramics and related compositions.[26−28] The enhancement in the piezoelectric properties was evident but not high enough. In the case of $BaTiO_3$ doped ceramics, BT, these have higher performance but have the drawback of low Curie temperature.[29,30] Nonetheless, we believe that there are still structural and electrical aspects that remain controversial with respect to the role of the phase coexistence induced by the compositional modifications in the KNN-based system, and, therefore, the enhancement of piezoelectric properties on such material should be closely related to this phase coexistence behavior.

The aim of this work is to study the ferro-piezoelectric properties of $0.96[(K_{0.48}Na_{0.52})_{0.95}Li_{0.05}Nb_{1-x}Sb_xO_3]$-0.04-$[BaZrO_3]$ lead-free ceramics ($KNLN_{1-x}S_x$-BZ) and to address effects that can give rise to d_{33} enhancement. To reach this objective, we present a facile method to design high-quality $KNLN_{1-x}S_x$-BZ lead-free ceramics, which is based on chemical modifications in the vicinity of a phase coexistence on the $(K_{0.5}Na_{0.5})NbO_3$-based system through the substitutions in the B-sites of the perovskite lattice by Sb^{5+} ions. This chemical modification resulted in the formation of a new phase boundary consisting of Rhombohedral and Tetragonal ($R-T$) phases, which greatly increase the electromechanical functionality. It should be emphasized that this material with the optimal phase coexistence can exhibit a significant high piezoelectric response with the d_{33} value as high as ∼400 pC/N, which is comparable to part soft PZTs and considerably higher than several established KNN-based lead-free systems.

2. EXPERIMENTAL DETAILS

Sample Preparation. The compositional ceramics of $0.96-[(K_{0.48}Na_{0.52})_{0.95}Li_{0.05}Nb_{1-x}Sb_xO_3]$-$0.04[BaZrO_3]$ (x = 0, 0.05, 0.06, 0.07, and 0.08), hereafter abbreviated as $KNLN_{1-x}S_x$-BZ, were prepared by a conventional solid-state reaction from an adequate mixture of corresponding oxides and carbonates. Na_2CO_3, Li_2CO_3 (J.T. Baker, >99.5%), K_2CO_3, $BaCO_3$ (Merck, >99% and >99%), Nb_2O_5, Ta_2O_5, and Sb_2O_5 (Sigma-Aldrich, >99.9%, >99%, and >99.995%, respectively) were used as starting raw materials. The amount of $BaZrO_3$ (BZ) was chosen due to BZ being a paraelectric phase with a cubic perovskite structure, which has been proven to be an excellent stabilizer for the R phase of the KNN-based system.[23,24] In all of the experiments, the raw materials were dried at 200 °C for 4 h before being used because of their hygroscopic nature.[31] These raw materials were weighed in the stoichiometric amounts and then mixed in an agate mortar and pestle using acetone. The mixture was then calcined at 850 °C for 4 h. The calcined powders were ball milled in a plastic jar with zirconia grinding media for 12 h in ethanol and dried for 4 h at 150 °C. Samples of 13 mm in diameter and 2 mm in thickness were uniaxially pressed at 260 MPa and sintered at 1120 °C for 4 h. Bulk densities of the samples were determined using the Archimedes method.

X-ray Diffraction (XRD). Crystalline phases were characterized by X-ray diffraction (XRD) (D8 Advance, Bruker, Germany), using CuK_α radiation, on powders obtained by milling the sintered ceramics. The patterns were recorded over the angular range 15−80° (2θ) with a step size of 0.0334° and a time per step of 100 s, using Cu K_α radiation (λ = 0.154056 nm) with working voltage and current of 40 kV and 100 mA, respectively. Structural refinement was performed using a tetragonal symmetry, (*T, P4mm*), an orthorhombic symmetry, (*O, Amm2*), and a rhombohedral symmetry, (*R, R3c*). The relative volume fractions can be calculated by using the integrated intensities of degenerate reflections, such as the tetragonal (002) and (200), orthorhombic (022) and (200), and rhombohedral (200) peak, respectively, obtained from line profile analysis.[9] Peaks positions were fit assuming a Lorentz peak shape. (*More information about the phase volume fraction vs Sb content is shown in* Supporting Information Figure S1.)

Electrical Properties. For the electrical measurements, silver pastes were coated on both sides of the sintered samples. After being fired at 600 °C for 30 min, these samples were used for characterizing electrical performance. In order to test the piezoelectric constant, the samples were polarized under a direct current (*dc*) electric field of 4 kV/mm in a silicon oil bath at 25 °C for 30 min.[32] Dielectric properties were determined at different temperatures and frequencies using an impedance analyzer HP4294A in the frequency range 100 Hz to 1 MHz.

The piezoelectric constant d_{33} was measured using a piezo d_{33} meter (YE2730A d_{33} METER, APC International, Ltd., USA) at temperatures between −10 and 250 °C. The transverse piezoelectric coefficient (d_{31}) and the planar coupling coefficient (k_p) were determined at room temperature by the resonance/antiresonance method on the basis of IEEE standards. The planar mechanical quality, Q_m, which is related to the sharpness of the resonance frequency, was calculated using the following equation[33]

$$Q_m = \frac{f_a^2}{2\pi f_r Z_m C^T (f_a^2 - f_r^2)} \quad (1)$$

where f_r is the resonance frequency (Hz), f_a is the antiresonance frequency (Hz), Z_m is the minimum impedance at f_r (ohm) resonance impedance, and C^T is the capacitance mechanically free at 1 kHz. Finally, the ferroelectric nature of these ceramics was determined using a hysteresis meter (RT 6000 HVS, RADIANT Technologies).

Raman Spectroscopy. Raman spectroscopy was carried out in the temperature range between −150 to 300 °C on sintered and polished pellets using a WITec Alpha-300R confocal Raman microscope with a 532 nm laser. A total of 20 measurements were done at different points for each temperature, to study the possible presence of secondary

DOI: 10.1021/acsami.5b06747
ACS Appl. Mater. Interfaces 2015, 7, 23080−23088

impurity phases because these could potentially emerge during sintering. Furthermore, investigation of the samples would allow comparing Raman spectra to dielectric measurements and piezoelectric properties on the search for potential multiphase coexistence, which would improve the functional response of the system. Collected spectra were analyzed by using Witec Control Plus Software, and Raman mode positions were fit assuming a Lorentz peak shape.

3. RESULTS AND DISCUSSION

3.1. Structural Characterization of the $KNLN_{1-x}S_x$-BZ Ceramics: Identification of the Polymorphic Behavior.

Figure 1 presents the X-ray diffraction patterns of $KNLN_{1-x}S_x$-BZ ceramics for different Sb^{5+} amounts sintered at 1120 °C for 4 h. All diffraction patterns correspond to a perovskite structure without secondary impurity phases in this system. In particular, the absence of secondary impurity phases, which is assigned to $K_6LiNb_6O_{17}$ (PDF# 36-0533) or $K_6Nb_{10.88}O_{30}$ (PDF# 87-1856) with tungsten-bronze type (TTB),[12] is a remarkable result because these TTBs phases are commonly present in sintered alkaline niobates and form liquid phases that affect piezoelectric response.[34] Two aspects are relevant to attain such behavior: First, Ta^{5+} cations are not incorporated, which commonly induce compositional inhomogeneities,[35] and, second, the incorporation of Ba^{2+} cations, as mineralizer, improves diffusion. Thus, the XRD patterns allow us to infer that the ceramic compositions under study form a stable solid solution.

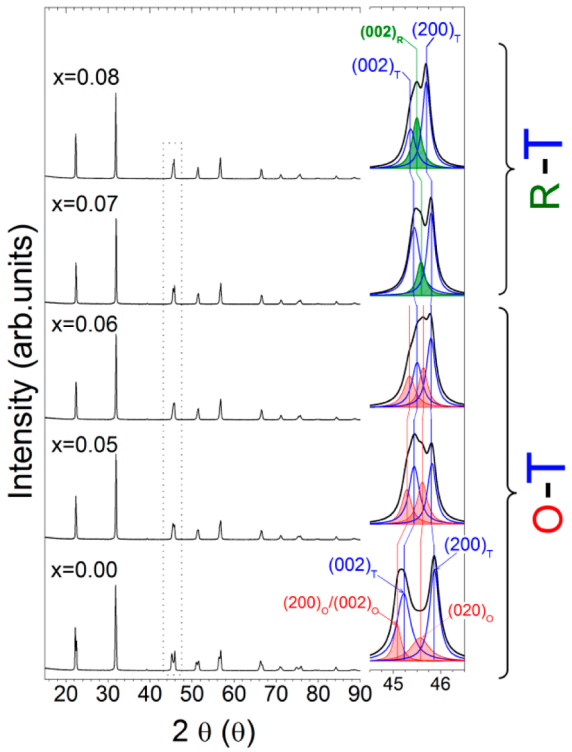

Figure 1. Identification of phase coexistence on the $KNLN_{1-x}S_x$-BZ ceramics by XRD: The figure shows X-ray diffraction patterns of $KNLN_{1-x}S_x$-BZ ceramics sintered at 1120 °C for 4 h. The inserts of each figure show a detail of the XRD diffraction pattern in the 2θ range 44.5° to 46.5° of the $KNLN_{1-x}S_x$-BZ ceramics. The patterns with x between 0.00 and 0.06 are fitted to the sum of four Lorentzian peaks, which are indexed as 2 tetragonal peaks (in blue color) plus 2 orthorhombic peaks (in red color) of the perovskite phase. While the ceramics with x between 0.07 and 0.08 were simulated to the sum of the three Lorentzian peaks, which are indexed as 2 tetragonal peaks (in blue color) plus the rhombohedral peak (in green color) of the perovskite phase (T: tetragonal symmetry, O: orthorhombic symmetry, and R: rhombohedral symmetry).

The inserts of Figure 1 display the splitting of the (200) pseudocubic peak into (200) and (002), which suggests a noncubic symmetry in these samples. The inserts show a detail of the XRD diffraction pattern in the 2θ range 44.5° to 46.5° of the $KNLN_{1-x}S_x$-BZ ceramic system as a function of the Sb^{5+} content. Moreover, as represented in the insets, the Sb^{5+} doping produces changes in the symmetry of the perovskite structure. All samples present the polymorphic behavior, which is associated with the room temperature coexistence between a tetragonal symmetry, (T, $P4mm$), an orthorhombic symmetry, (O, $Amm2$), and a rhombohedral symmetry, (R, $R3c$). The coexistence of different polymorphs (tetragonal and orthorhombic phases) was previously reported on KNL-NTS bulk ceramics.[8,12,16,22,32,35−38] Furthermore, the above behavior shows a clear dependence on the Sb^{5+} content (see the insert of Figure 1).

As a result, the ceramics with $0.00 \leq x \leq 0.06$ have a coexistence of $O-T$ phases,[39] being more relevant to the peaks associated with T symmetry. However, we can detect that there is a different trend for the ceramics with high Sb^{5+} content ($0.07 \leq x \leq 0.08$). In the compositional range $0.07 \leq x \leq 0.08$, the XRD patterns could not be indexed with either T or O structures. Structural refinement resulted in a new phase coexistence at room temperature, consistent with a mixed ($R + T$) phase structure containing both polarization directions (see the insert of Figure 1). This fact confirms that compounds in this region also are polar at room temperature. The concomitant observation of the XRD diffraction pattern characteristic of the KNN-based rhombohedral polymorph allows thinking that this local structure is probably of rhombohedral symmetry (although the monoclinic structure (M, Pm, or Cm) is not disregarded), thus with polarization along the $\langle 111 \rangle_{pc}$ direction. This agrees well with the recently reported observation by high energy synchrotron XRD diffraction measurements of the local structure of monoclinic symmetry in KNN ceramics.[40] In this last case, also the more relevant phase is the T phase. As a consequence, the most probable origin of this behavior must be related to the solubility of Sb^{5+} ions into the perovskite structure. So, we suppose that the gradual entry of Sb^{5+} ions into the KNLN-BZ perovskite lattice produces an evolution in multiphase coexistence suppressing the O phase in favor of the R phase.

3.2. Determination of the Phase Transition Temperatures.

To verify that the polymorphic behavior is influenced by Sb^{5+} doping on the KNN-based system, additional experiments were performed from their dielectric permittivity (ε') vs T curves (see Figure 2). So, the $\varepsilon'-T$ curves of each sample were measured in the temperature range of 25−400 °C, as shown in Figure 2a. Figure 2a shows the temperature dependence of the dielectric permittivity ε' (at 100 kHz) of $KNLN_{1-x}S_x$-BZ ceramics as a function of x. It is well-known that in the KNN-based system there are four polymorphic phases, rhombohedral (R), orthorhombic (O), tetragonal (T), and cubic (C) phases, with increasing temperature. So, the transition temperatures are correspondingly defined as T_{R-O}, T_{O-T}, and T_C (or Curie temperature). The curves corresponding to ceramics with $0.00 \leq x \leq 0.06$ present two transitions (see the curves marked as **1**, **2**, and **3** in Figure 2a), which are associated with the corresponding T_{O-T} and T_C, respectively. In

DOI: 10.1021/acsami.5b06747
ACS Appl. Mater. Interfaces 2015, 7, 23080−23088

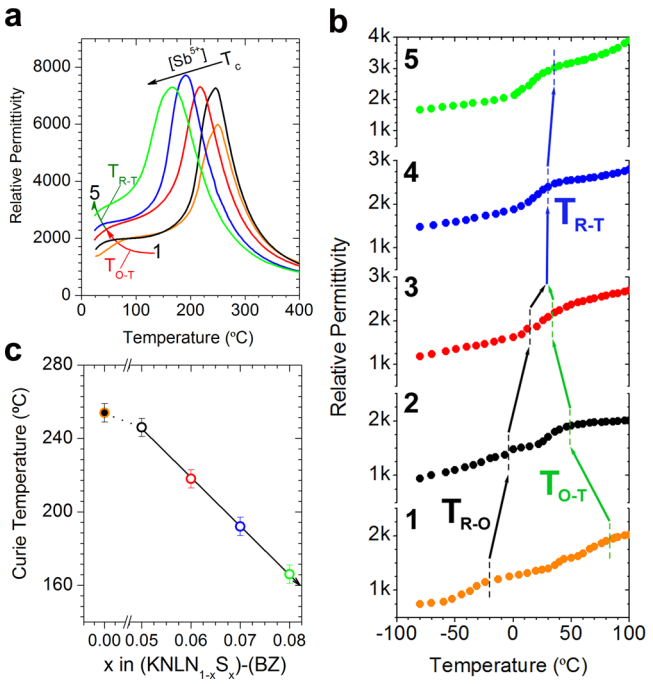

Figure 2. Influence of the Sb^{+5} on phase transitions of the $KNLN_{1-x}S_x$-BZ ceramics. Panel a shows real permittivity (ε') vs temperature of $KNLN_{1-x}S_x$-BZ sintered ceramics (at 100 kHz). Panel b shows a detail of the ε_r−T curves of $KNLN_{1-x}S_x$-BZ ceramics in the temperature range −80 to 100 °C. Panel c shows the evolution of the T_c of the $KNLN_{1-x}S_x$-BZ ceramics as a function of the Sb^{5+} content (the sensitivity of the phase transition temperatures, T_c, was estimated as ±5 °C). The ceramic compositions represented in panels a and b are the following: (**1**) x = 0.00; (**2**) x = 0.05; (**3**) x = 0.06; (**4**) x = 0.07; and (**5**) x = 0.08. The arrows marked in panel a correspond to the T_{R-T}, T_{O-T}, and T_C evolution, while the arrows marked in panel b correspond to the T_{R-O}, T_{O-T}, and T_{R-T} depending on compositions.

the temperature range studied, only T_C can be detected for ceramics with high Sb^{5+} content (see the curves marked as **4** and **5** of Figure 2a). This means that the polymorphic phase transition assigned to $R-T$ coexistence detected by XRD takes place below and/or close to room temperature.

To clearly compare the evolution of the phase structure, we choose the ε'−T curves of $KNLN_{1-x}S_x$-BZ ceramics in the temperature range −80 to 100 °C to determinate the variations of both T_{O-T} and T_{R-O}, as shown in Figure 2b. We can clearly observe from Figure 2b that the addition of Sb^{5+} decreases T_{O-T} and increases T_{R-O} simultaneously, which results in the formation of the $R-T$ phase boundary for a high doping range ($x \geq 0.07$). Considering the results of both XRD patterns and ε'−T curves [see Figures 1 and 2a], two situations can be identified depending on the doping content: First, for a low doping range, the ceramics belong to the O and T phase coexistence close to room temperature; and, second, for a high doping range, the $O-T$ phase boundary is suppressed in favor of a new $R-T$ phase transition, which is below and/or close to room temperature, depending on the x content.

On the other hand, we also focus on the variation of T_C with Sb^{5+} content, and this has been plotted in Figure 2c. As compared with the $KNLN_{1-x}S_x$-BZ ceramics without Sb^{5+} we notice that the ceramics with Sb^{5+} have a lower T_C, which shows a linear relationship with the Sb^{5+} content. This phenomenon is consistent with previously reported results in KNN with the addition of other B-site doping.[22,39,41−44] Moreover, the dielectric constant value at the T_c increases with the Sb^{5+} doping, reaching a maximum at x = 0.07. Noteworthy, the dielectric constant at room temperature increases with the doping amount, while the dielectric losses remain low (see Table S1, Supporting Information). The coexistence of $R-T$ phases increases the charge accumulation of the system. This behavior is similar to the one that occurs at the MPB in the PZT system. This fact anticipates the improvement of the piezoelectric properties.

3.3. Influence of the Phase Transition at Room Temperature on the Functional Properties of the $KNLN_{1-x}S_x$-BZ Ceramics. The high density $KNLN_{1-x}S_x$-BZ ceramics are perfectly adapted to measure the ferroelectric functionality and to try to correlate such properties to the observed structural evolution. For a better understanding of the relationship between physical-chemical phenomena and electromechanical properties of the ceramics, the dependence polarization (P-E) loops as a function of Sb^{5+} content were measured, as displayed in Figure 3. From Figure 3a, we can observe that all the ceramics exhibit good square hysteresis loops at room temperature, revealing their ferroelectric character. As it is observed in the inset of Figure 3a the coercive field (E_c) decreases almost linearly with the Sb^{5+} content evidencing that the ferroelectricity is clearly sensitive to the Sb^{5+} content. To make clear the effects of Sb^{5+} content on

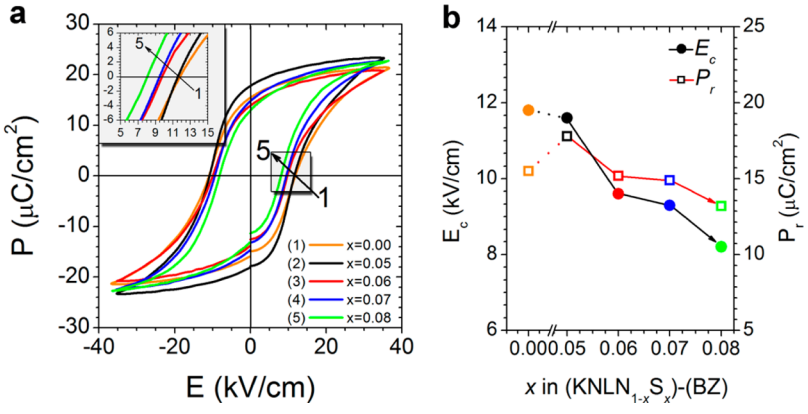

Figure 3. Ferroelectric behaviors of the $KNLN_{1-x}S_x$-BZ ceramics: panel a $P-E$ loops and panel b P_r and E_c values of the ceramics as a function of the x. The insert of panel a shows a detail of the E_c evolution. The ceramic compositions represented in panel a are the following: (**1**) x = 0.00; (**2**) x = 0.05; (**3**) x = 0.06; (**4**) x = 0.07; and (**5**) x = 0.08.

DOI: 10.1021/acsami.5b06747
ACS Appl. Mater. Interfaces 2015, 7, 23080−23088

the ferroelectric behavior of the system, the remnant polarization (P_r) and coercive field (E_c) of each sample derived from Figure 3a are plotted in Figure 3b. In this figure is observed that both P_r and E_c decrease as the Sb^{5+} content increases, and this behavior has been reported for similar compositions.[21,39,45] The decrease in E_c indicates that the addition of Sb^{5+} facilitates the movement of ferroelectric domain and made the polarization switching easier (softening effect).

Keeping in mind that these materials can be used in devices operating at room temperature, an important aspect to consider is the design of the phase transition at room temperature. Thus, T_{O-T} and T_{R-T} should be controlled for a high d_{33} value in KNN-based ceramics. Besides, it is well-known that dielectric and ferroelectric properties determine the piezoelectric properties; remember that the d_{33} piezoelectric constant is proportional to the $\varepsilon_r P_r$ product.[39,45] Then, even though the P_r is relative low, the ε' is high, and then the piezoelectric properties increase. The high dielectric permittivity is related to the coexistence of the $R-T$ phases, which make the system (sample) more polarizable due to the existence of more directions for the polarization orientation, and more importantly it provides the rotation path for the enhanced piezoelectric properties near the phase boundary.[46−48] This fact is highly remarked by the appearance of large P_s (*saturation polarization*) values for the compositions having rhombohedral−tetragonal coexistence at room temperature. The large P_s in spite of the lower values of the P_r indicates a high domain mobility characteristic of donor doped piezoceramics.

To examine the piezoelectric behavior, samples were poled, and longitudinal piezoelectric coefficients (d_{33}) were measured across the full range of compositions ($0 \le x \le 0.08$). The behavior of the d_{33} piezoelectric constant versus $\varepsilon_r P_r$ product is shown in Figure 4. Compositions with coexistence of the $O-T$ phases, $0.00 \le x \le 0.06$ (blue area of Figure 4), show an increase in d_{33} with increasing x, reaching a maximum of 315 $pC{\cdot}N^{-1}$ at $x = 0.06$. The most relevant result obtained from the d_{33} evolution is the substantial increase near the morphotropic phase boundary (green area of Figure 4), which reaches a maximum d_{33} of ~400 $pC{\cdot}N^{-1}$ for $x = 0.07$. This represents an improvement of 25% regarding that found for O and T coexistence (315 $pC{\cdot}N^{-1}$ at $x = 0.06$). The high d_{33} value is similar to that of soft PZT (425 $pC{\cdot}N^{-1}$)[33] and is considerably higher than several established KNN-based lead-free systems (244−360 $pC{\cdot}N^{-1}$)[37,38,49,50] (see Table S1, Supporting Information). The $\varepsilon_r P_r$ increases as the Sb^{5+} content increases; this is because of the coexistence of the rhombohedral−tetragonal phases beginning to appear, reaching a maximum at $x = 0.07$. The phase coexistence means that polarization can adopt 14 directions (6 from the tetragonal phase and 8 from the rhombohedral phase, respectively); these results confirm the dielectric data discussed above. So, the higher the $\varepsilon_r P_r$ product the higher the piezoelectric properties, and the maximum value is shown for $x = 0.07$ of Sb^{5+} content, which yield a d_{33} value as high as ~400 $pC{\cdot}N^{-1}$ at room temperature. On the other hand, at this stage one drawback is the low T_c of the 0.07 composition.

Summarizing, the piezoelectric properties present a clear relationship with the phase coexistence at room temperature (Figure 4). Logically and as for P_r, the piezoelectric properties are governed by the stabilization of a Rhombohedral−Tetragonal ($R-T$) phase boundary close to room temperature, which enhances the polarization process of the system.

The transverse piezoelectric coefficient (d_{31}), the planar coupling coefficient (k_p), and the mechanical quality factor (Q_m) were calculated from radial extensional resonance mode on poled disks as shown in Figure 5 a-b. It is seen that both piezoelectric charge constants, d_{33} and d_{31}, increase progressively with increasing the Sb^{5+} content and reach a maximum at $x = 0.07$ Sb^{5+} due to the phase coexistence discussed above. The k_p has a similar trend, i.e. increases slightly with increasing Sb^{5+}, and reaches its top value close to $x = 0.07$

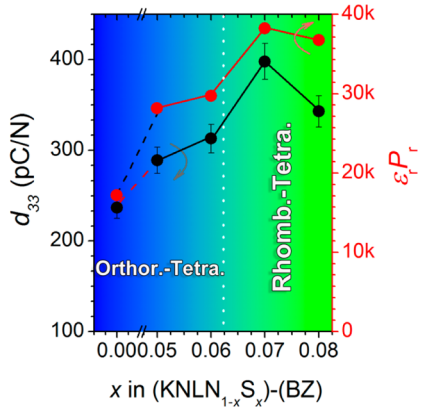

Figure 4. Detection of a high d_{33} value on the $KNLN_{1-x}S_x$-BZ ceramics at room temperature: d_{33} and $\varepsilon_r P_r$ vs Sb^{5+} content on the $KNLN_{1-x}Sb_x$-BZ system. The blue and green areas delimit the compositional regions where is located the coexistence of the $O-T$ and $R-T$ phases of the $KNLN_{1-x}Sb_x$-BZ system, respectively. The white dotted line limits the two phase boundaries involved in the $KNLN_{1-x}Sb_x$-BZ system. The standard tolerance for the electrical properties is ±10%.

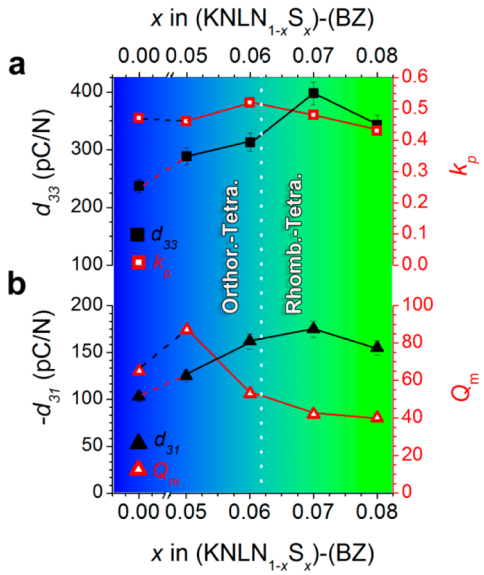

Figure 5. Dielectric and piezoelectric properties at room temperature of the $KNLN_{1-x}S_x$-BZ ceramics as a function of the Sb^{5+} content: panel a d_{33} and k_p as well as panel b d_{31} and Q_m of the ceramics as a function of Sb^{5+} content. The blue and green areas delimit the compositional regions where is located the coexistence of the $O-T$ and $R-T$ phases of the $KNLN_{1-x}Sb_x$-BZ system, respectively. The white dotted line limits the two phase boundaries involved in the $KNLN_{1-x}Sb_x$-BZ system. *Data are measured at 25 °C and 24 h after poling.* The standard tolerances for the electrical and electromechanical properties are ±10% and ±5%, respectively.

DOI: 10.1021/acsami.5b06747
ACS Appl. Mater. Interfaces 2015, 7, 23080−23088

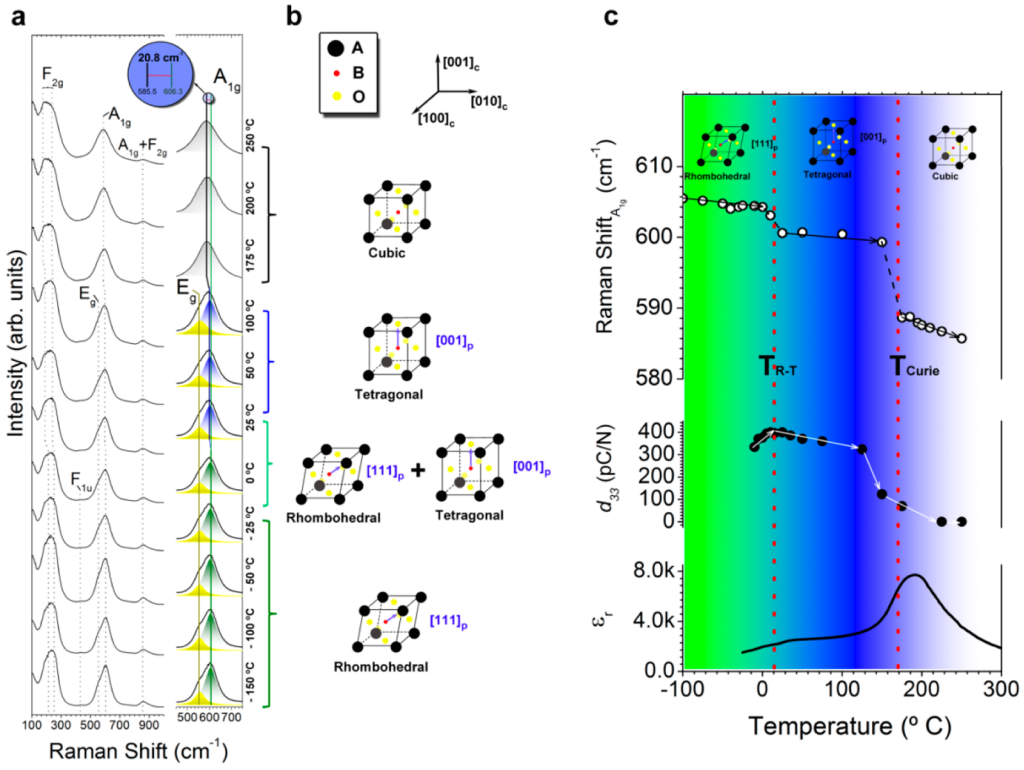

Figure 6. Temperature dependence on the phase transitions and its influence on the piezoelectric properties of the $KNLN_{1-x}S_x$-BZ ceramic with composition $x = 0.07$: Panel a shows the sequence of average Raman spectra showing the evolution of the phase transition in the $KNLN_{1-x}S_x$-BZ ceramic with composition $x = 0.07$ for different temperatures between −150 °C → 250 °C. These Raman spectra are fitted to the sum of two Lorentzian peaks, ascribed to the E_g (υ_2) and A_{1g} (υ_1) corresponding to Raman modes of the perovskite phase. Moreover, the inset in the top of panel a shows an enlargement of the A_{1g} Raman shift taken between the temperatures at −150 and 250 °C, exhibiting a decrease Raman shift of 20.8 cm^{-1}. Panel b shows the schematic polarization rotation process in a perovskite unit cell ABO_3, from the rhombohedral (R) phase to the cubic (C) phase, whereby the polarizations are represented by blue arrows. The Raman shift evolution of the A_{1g} Raman mode is plotted as a function of the temperature in the panel c. As a comparison and to evaluate the influence of the phase transitions on the functional properties, panel c also represents the longitudinal piezoelectric coefficients (d_{33}) and dielectric permittivity (ε') evolution vs temperature. From panel c, high piezoelectric activity is observed for the phase coexistence optimal between a rhombohedral (R) and a tetragonal symmetry (T) close to room temperature. The red dotted lines limit the phase transitions involved in the $KNLN_{1-x}Sb_x$-BZ system, which are driven by temperature.

and then decreases again. Thus, for $x = 0.07$ ($R-T$ phase coexistence), d_{31}, k_p, and Q_m are 175 $pC{\cdot}N^{-1}$, 0.48, and 42, respectively (see Table S1, Supporting Information for the other compositions under study and comparison with soft PZT). As a relevant result, the $R-T$ phase coexistence improves the piezoelectric activity, while the $O-T$ phase boundary increases the mechanical quality factor, Q_m. To better understand the influence of multiphase coexistence on the functional properties of the system, we performed the relative volume fractions investigations by X-ray diffraction (XRD). *The reader can find more information about the relative volume fractions vs* Sb^{5+} *in* Supporting Information Figure S1.

3.4. Temperature Dependence on the Phase Transitions: Revealing the Role of Multiphase Coexistence in Improving the Piezoelectric Properties. Considering that the enhanced piezoelectric property of $KNLN_{1-x}S_x$-BZ ceramics is comprehensively assumed to be the existence of a rhombohedral−tetragonal coexistence phase, and keeping in mind that Raman spectroscopy is sensitive to phase transitions in ceramic materials, we used confocal Raman spectroscopy to monitor the distortion of the oxygen octahedra for the ceramic with $x = 0.07$. The ($R-T$ phase coexistence) composition $x = 0.07$ was selected for a detailed study of structural evolution vs temperature, and, therefore, we try to know whether the $R-T$ phase coexistence could be driven further improving its temperature stability of the system. The vibrations of the BO_6 octahedron consist of $1A_{1g}$ (υ_1) + $1E_g$ (υ_2) + $2F_{1u}$ (υ_2, υ_4) + F_{2g} (υ_5) + F_{2u} (υ_6) modes. Of these vibrations, $1A_{1g}$ (υ_1) + $1E_g$ (υ_2) + $1F_{1u}$ (υ_3) are stretching modes and the rest, bending modes.[51,52] In particular, A_{1g} (υ_1) symmetrical mode and F_{2g} (υ_5) antisymmetric mode are detected as relatively strong scattering signals in KNN-based materials because of a near-perfect equilateral octahedral symmetry. A series of temperature dependent average Raman spectra of the $KNLN_{1-x}S_x$-BZ ceramics with $x = 0.07$ is shown in Figure 6a. The spectra are focused on the mixed E_g (υ_2) and A_{1g} (υ_1) in the 450−750 cm^{-1} frequency range, see insert of Figure 6a. Clearly, a continuous decrease in the Raman shift of the A_{1g} mode occurs when temperature increases from −150 to 250 °C of the ceramic with $x = 0.07$. This behavior observed here implies a modification of the polarization direction, at least at a local scale. The Raman shift is also an indicator of the crystal stress and correlates with the polarization.[8,16,52] Indeed, a modification of the chemical environment (atomic displacement, local stress, ...) changes the force constants of chemical bonds and thus modifies the phonon frequency of some Raman modes (Raman shift). By analogy with the visible spectrum and compared to reference, a frequency increase of the Raman peak frequency is called "blueshift" (higher energy of phonon), while a frequency decrease is called "redshift". The redshift of the A_{1g}

DOI: 10.1021/acsami.5b06747
ACS Appl. Mater. Interfaces 2015, 7, 23080−23088

Raman mode (insert in the top of Figure 6a) indicates a structural change as a consequence of the polarization rotation produced by phase transitions of the system. Additionally, on the right of each temperature range and associated with each one of the structural modifications is displayed the schematic polarization rotation process in a perovskite unit cell ABO_3, from the rhombohedral (R) phase to the cubic (C) phase (Figure 6b).

To make clear the temperature effect on the structural changes of the system, the Raman shift of the A_{1g} mode of each temperature derived from Figure 6a is plotted in Figure 6c. It is worth noticing a characteristic aspect in the A_{1g} Raman shift evolution, which demonstrates two abrupt discontinuities; the first one occurs at temperatures between 0° and 25 °C and is due to the $R-T$ phase transition. The second one, associated with the $T-C$ phase transition (*Curie temperature,* T_C), occurs around ∼175 °C. This last phase transition is easily detectable since it is characterized by the annihilation of the E_g Raman mode, as shown in the top of the inset of Figure 6a. It is well established, that while ideally the Raman modes of a perovskite unit cell ABO_3 should completely disappear above T_C, they usually only decrease in magnitude and broaden indicating that the symmetry of the paraelectric phase is *pseudocubic* instead of the previously reported cubic phase. This behavior can be possibly explained due to an order−disorder transition component and local deviations from the ideal structure. Raman spectroscopy is based on bond polarization, and, in this case, we observe the main vibrations associated with the BO_6 perovskite-octahedron. As a consequence, the presence of active Raman modes above T_C could provoke partial retention of the polarization at a local scale.

Generally speaking, the properties of ferroelectric materials are governed by the occurrence of electric dipole moments in piezoelectric/ferroelectric materials, in which the application of an electrical field creates mechanical deformation or vice versa.[53] Thus, piezoelectric lattice-deformations are inevitably associated with polarization variations. In Figure 6b and associated with each temperature range has been represented a schematic process of the polarization rotation in a perovskite unit cell ABO_3, from its rhombohedral (R) state to its cubic (C) state, which passes through a phase coexistence state between a rhombohedral (R) and a tetragonal (T) state close to room temperature. The most relevant result obtained from the Raman characterization of the ceramic with $x = 0.07$ is the confirmation of this new $R-T$ phase transition, which depends on the x content, and it has been demonstrated by XRD and $\varepsilon'-T$ curves. The construction of this phase coexistence induces in the system a high degree of polarization directions close to room temperature, associated with the spontaneous polarization reorientation on the $[111]_c$ and $[001]_c$ direction for the rhombohedral (R) and tetragonal (T) phases, respectively. Thus, the $R-T$ phase coexistence at room temperature produces a lattice-deformation associated with the high degree of the polarization directions that contribute to the domain mobility and therefore to the enlargement of the piezoelectric properties.

Figure 6c summarizes the temperature dependence on the Raman shift evolution of the A_{1g} Raman mode (*top*), piezoelectric charge coefficient d_{33} (*middle*), and dielectric properties (*bottom*) of the $KNLN_{1-x}S_x$-BZ ceramics with $x = 0.07$ in the temperature range −100 to 250 °C. From Figure 6c, it is found that coexistence of rhombohedral and tetragonal phases for the $x = 0.07$ composition exhibits an anomaly in all of the properties close to room temperature, as previously introduced in Figures 1, 4, and 5. Figure 6c (*middle*) shows the most interesting result to be a high value of ∼400 $pC{\cdot}N^{-1}$ for the piezoelectric coefficient d_{33}. (More information about the d_{33} evolution vs temperature can be found in Supporting Information Figure S2).

Taking into account the above results, we have demonstrated that the piezoelectric activity of $KNLN_{1-x}S_x$-BZ ceramics, with $x = 0.07$, can be comparable to part soft PZTs. In analogy with the PZT system, the coexistence of the rhombohedral and tetragonal phases occurs, the resulting large dielectric constant favors the ferroelectric domain mobility, and, as a consequence, the macroscopic property coefficients are also maximized. However, there are a number of critical observations associated with our findings: first, the temperature restrictions in which room temperature allows the maximum piezoelectric constant and, second, the relative low T_c (∼175 °C) for the ceramic with $x = 0.07$, as shown in Figure 2. In the origin of the $R-T$ coexistence, we make also evident that a remarkable contribution on the system under study is the absence of secondary impurity phases. The secondary impurity phase appearance is commonly observed in many of the alkaline niobate based piezoceramics.[12,34,54] Considering that the role of the secondary impurity phase is the partial retention of the alkali elements into its crystalline structure during the sintering step, this promotes the displacement of the alkaline elements from the main perovskite phase. In particular the secondary impurity phases are Li and K rich phases. As a consequence, we reported recently that this fact plays a crucial role in the phase transition temperatures of the alkaline niobate based system.[54] Thus, the system proposed here shows noticeable advantages over other KNN-based lead-free systems: first, the absence of secondary impurity phases allows tuning the tetragonality ratio by the control of Sb^{5+} content; second, the incorporation of $BaZrO_3$ is the key point to promote the appearance and stabilization of a rhombohedral phase; and, last but not least, the absence of tantalum cations in the composition contributes to the homogeneity and to the reduction of the complexity of the system. As tantalum oxide, Ta_2O_5, is scarce and expensive, the addition of Ta^{5+} should be avoided as far as possible or be used with a low content in terms of their practical applications. Thus, tantalum oxide-free compositions proposed here will contribute greatly to the development of the lead-free piezoceramics with large piezoelectric properties.

4. CONCLUSIONS

The implication derived from this study is that we can surprisingly modulate the multiphase coexistence of the $0.96[(K_{0.48}Na_{0.52})_{0.95}Li_{0.05}Nb_{1-x}Sb_xO_3]$-$0.04[BaZrO_3]$ lead-free system by replacement of the B-sites with Sb ions in the perovskite structure. So, we have stabilized a perovskite structure with a new phase boundary consisting of Rhombohedral and Tetragonal ($R-T$) phases, which is accessible at room temperature. The mixed phase region induces in the system a high degree of polarization directions close to room temperature, associated with the polarization directed along the $[001]_p$ and $[111]_p$ primitive cell edges for the rhombohedral (R) and tetragonal (T) phases, respectively. Thus, the $R-T$ phase coexistence at room temperature produces a lattice-deformation associated with the high degree of the polarization directions that contribute to the domain mobility and therefore to the enlargement of the piezoelectric properties. Based on these results, the $R-T$ mixed phase region develops a

DOI: 10.1021/acsami.5b06747
ACS Appl. Mater. Interfaces 2015, 7, 23080−23088

significant high piezoelectric response with a d_{33} value as high as ~400 pC/N, which is comparable to part soft PZTs. This knowledge should be used in the design of new lead-free piezoceramics with superior property coefficients and functionalities, pointing out that these compounds should be seriously considered as candidates for the substitution of PZT.

■ ASSOCIATED CONTENT

Supporting Information

The Supporting Information is available free of charge on the ACS Publications website at DOI: 10.1021/acsami.5b06747.

Composition dependence on the volume fraction for tetragonal (T), orthorhombic (O), and rhombohedral (R) phases; Temperature dependence on the piezoelectric charge coefficient (d_{33}) taken between −25 and 100 °C; Schematic polarization rotation process in a perovskite unit cell ABO_3, from rhombohedral (R) to tetragonal (T) state; Density (ρ), electrical, mechanical, and electromechanical properties of $KNLN_{1-x}Sb_x$-BZ ceramics at room temperature (PDF)

■ AUTHOR INFORMATION

Corresponding Authors

*E-mail: frmacos@icv.csic.es (F.R.-M.). Address correspondence and requests for materials.

*E-mail: rlopez@iim.unam.mx (R.L.-J.). Address correspondence and requests for materials.

Author Contributions

‖F. Rubio-Marcos and R. López-Juárez contributed equally.

Notes

The authors declare no competing financial interest.

■ ACKNOWLEDGMENTS

F.R.-M., R.E.R.-H., A.d.C., and J.F.F. express their thanks to the MINECO (Spain) project MAT2013-48009-C4-1-P for their financial support. Dr. F. Rubio-Marcos is also indebted to MINECO for a "'Juan de la Cierva"' contract (ref: JCI-2012-14521), which is cofinanced with European Social Found.. R. López-Juárez kindly acknowledges CONACyT and DGAPA for their financial support under projects CB-2011-1 No.166108 and PAPIIT IN102715, respectively.

■ REFERENCES

(1) Cross, E. Materials Science: Lead-Free at Last. *Nature* **2004**, *432*, 24−25.

(2) http://ec.europa.eu/environment/waste/weee/index_en.htm (accessed 21 January 2011).

(3) Takenaka, T.; Nagata, H. Current Status and Prospects of Lead-Free Piezoelectric Ceramics. *J. Eur. Ceram. Soc.* **2005**, *25*, 2693−2700.

(4) Shrout, T. R.; Zhang, S. J. Lead Free Piezoelectric Ceramics: Alternatives for PZT? *J. Electroceram.* **2007**, *19*, 111−124.

(5) Rödel, J.; Jo, W.; Seifert, K. T. P.; Anton, E. M.; Granzow, T.; Damjanovic, D. Perspective on the Development of Lead-Free Piezoceramics. *J. Am. Ceram. Soc.* **2009**, *92*, 1153−1177.

(6) Levin, I.; Reaney, I. M. Nano- and Mesoscale Structure of $Na_{1/2}B_{1/2}TiO_3$: A TEM Perspective. *Adv. Funct. Mater.* **2012**, *22*, 3445−3452.

(7) Schütz, D.; Deluca, M.; Krauss, W.; Feteira, A.; Jackson, T.; Reichmann, K. Lone-Pair-Induced Covalency as the Cause of Temperature- and Field-Induced Instabilities in Bismuth Sodium Titanate. *Adv. Funct. Mater.* **2012**, *22*, 2285−2294.

(8) Bortolani, F.; Campo, A.; Fernandez, J. F.; Clemens, F.; Rubio-Marcos, F. High Strain in $(K,Na)NbO_3$-based Lead-Free Piezoelectric Fibers. *Chem. Mater.* **2014**, *26* (12), 3838−3848.

(9) Ge, W.; Li, J.; Viehland, D.; Chang, Y.; Messing, G. L. Electric-Field-Dependent Phase Volume Fractions and Enhanced Piezoelectricity Near the Polymorphic Phase Boundary of $(K_{0.5}Na_{0.5})_{1-x}Li_xNbO_3$ Textured Ceramics. *Phys. Rev. B: Condens. Matter Mater. Phys.* **2011**, *83*, 224110.

(10) Saito, Y.; Takao, H.; Tani, T.; Nonoyama, T.; Takatori, K.; Homma, T.; Nagaya, T.; Nakamura, M. Lead-Free Piezoceramics. *Nature* **2004**, *432*, 84−87.

(11) Wang, K.; Li, J.-F. Domain Engineering of Lead-Free Li-Modified $(K,Na)NbO_3$ Polycrystals with Highly Enhanced Piezoelectricity. *Adv. Funct. Mater.* **2010**, *20*, 1924−1929.

(12) Rubio-Marcos, F.; Ochoa, P.; Fernández, J. F. Sintering and Properties of Lead-Free Piezoceramics. *J. Eur. Ceram. Soc.* **2007**, *27* (13), 4125−4129.

(13) Saito, Y.; Takao, H. Synthesis of Polycrystalline Platelike $KNbO_3$ Particles by the Topochemical Micro-Crystal Conversion Method and Fabrication of Grain-Oriented $(K_{0.5}Na_{0.5})NbO_3$ Ceramics. *J. Eur. Ceram. Soc.* **2007**, *27*, 4085−4092.

(14) Guo, Y.; Kakimoto, K. I.; Ohsato, H. Phase Transitional Behavior and Piezoelectric Properties of $(Na_{0.5}K_{0.5})NbO_3$−$LiNbO_3$ Ceramics. *Appl. Phys. Lett.* **2004**, *85*, 4121.

(15) Zhu, W.; Zhu, J.; Wang, M.; Zhu, B.; Zhu, X.; Pezzotti, G. Raman Tensor Analysis of $(K_{0.5}Na_{0.5})NbO_3$−$LiSbO_3$ Lead-Free Ceramics and its Application to Study Grain/Domain Orientation. *J. Raman Spectrosc.* **2012**, *43*, 1320−1328.

(16) Rubio-Marcos, F.; Del Campo, A.; López-Juárez, R.; Romero, J. J.; Fernández, J. F. High Spatial Resolution Structure of $(K,Na)NbO_3$ Lead-Free Ferroelectric Domains. *J. Mater. Chem.* **2012**, *22*, 9714−9720.

(17) Venkatesh, J.; Sherman, V.; Setter, N. Synthesis and Dielectric Characterization of Potassium Niobate Tantalate Ceramics. *J. Am. Ceram. Soc.* **2005**, *88*, 3397−3404.

(18) Vendrell, X.; García, J. E.; Rubio-Marcos, F.; Ochoa, D. A.; Mestres, L.; Fernández, J. F. Exploring Different Sintering Atmospheres to Reduce Nonlinear Response of KNN-Modified Piezoceramics. *J. Eur. Ceram. Soc.* **2013**, *33*, 825−831.

(19) Wang, X.; Wu, J.; Xiao, D.; Cheng, X.; Zheng, T.; Zhang, B.; Lou, X.; Zhu, J. Large d_{33} in (K,Na) $(Nb,Ta,Sb)O_3$-$(Bi,Na,K)ZrO_3$ Lead-Free Ceramics. *J. Mater. Chem. A* **2014**, *2*, 4122−4126.

(20) Wang, X.; Wu, J.; Xiao, D.; Cheng, X.; Zheng, T.; Zhang, B.; Lou, X.; Zhu, J. New Potassium−Sodium Niobate Ceramics with a Giant d_{33}. *ACS Appl. Mater. Interfaces* **2014**, *6*, 6177−6180.

(21) Wang, X.; Wu, J.; Xiao, D.; Zhu, J.; Cheng, X.; Zheng, T.; Zhang, B.; Lou, X.; Wang, X. Giant Piezoelectricity in Potassium−Sodium Niobate Lead-Free Ceramics. *J. Am. Chem. Soc.* **2014**, *136*, 2905−2910.

(22) Wu, J.; Xiao, D.; Zhu, J. Potassium−Sodium Niobate Lead-Free Piezoelectric Materials: Past, Present, and Future of Phase Boundaries. *Chem. Rev.* **2015**, *115* (7), 2559−2595.

(23) Zuo, R.; Fu, J. Rhombohedral-Tetragonal Phase Coexistence and Piezoelectric Properties of (NaK) $(NbSb)O_3$-$LiTaO_3$-$BaZrO_3$ Lead-Free Ceramics. *J. Am. Ceram. Soc.* **2011**, *94* (5), 1467−1470.

(24) Fu, J.; Zuo, R.; Wu, S. C.; Jiang, J. Z.; Li, L.; Yang, T. Y.; Wang, X.; Li, L. Electric Field Induced Intermediate Phase and Polarization Rotation Path in Alkaline Niobate Based Piezoceramics Close to the Rhombohedral and Tetragonal Phase Boundary. *Appl. Phys. Lett.* **2012**, *100*, 122902.

(25) Ochoa, D. A.; Garcia, J. A.; Perez, R.; Gomis, V.; Albareda, A.; Rubio-Marcos, F.; Fernandez, J. F. Extrinsic Contributions and Nonlinear Response in Lead-Free KNN-Modified Piezoceramics. *J. Phys. D: Appl. Phys.* **2009**, *42*, 025402.

(26) Zhang, S.; Xia, R.; Shrout, T. R. Modified $(K_{0.5}Na_{0.5})NbO_3$ Based Lead-Free Piezoelectrics with Broad Temperature Usage Range. *Appl. Phys. Lett.* **2007**, *91* (13), 132913.

(27) Wu, J. G.; Xiao, D. Q.; Wang, Y. Y. $CaTiO_3$-modified $[(K_{0.5}Na_{0.5})_{0.94}Li_{0.06}](Nb_{0.94}Sb_{0.06})O_3$ Lead-Free Piezoelectric Ce-

DOI: 10.1021/acsami.5b06747
ACS Appl. Mater. Interfaces 2015, 7, 23080−23088

ramics with Improved Temperature Stability. *Scr. Mater.* **2008**, *59*, 750−752.
(28) Wu, J. G.; Xiao, D. Q.; Wang, Y. Y.; Zhu, J. G. Improved Temperature Stability of $CaTiO_3$-Modified $[(K_{0.5}Na_{0.5})_{0.96}Li_{0.04}]$-$(Nb_{0.91}Sb_{0.05}Ta_{0.04})O_3$ Lead-Free Piezoelectric Ceramics. *J. Appl. Phys.* **2008**, *104*, 024102.
(29) Ehmke, M. C.; Ehrlich, S. N.; Blendell, J. E.; Bowman, K. J. Phase Coexistence and Ferroelastic Texture in High Strain (1-x)$Ba(Zr_{0.2}Ti_{0.8})O_3$-x$(Ba_{0.7}Ca_{0.3})TiO_3$ Piezoceramics. *J. Appl. Phys.* **2012**, *111*, 124110.
(30) Liu, W.; Ren, X. Large Piezoelectric Effect in Pb-Free Ceramics. *Phys. Rev. Lett.* **2009**, *103*, 257602.
(31) Bomlai, P.; Wichianrat, P.; Muensit, S.; Milne, S. J. Effect of Calcination Conditions and Excess Alkali Carbonate on the Phase Formation and Particle Morphology of $Na_{0.5}K_{0.5}NbO_3$ Powders. *J. Am. Ceram. Soc.* **2007**, *90*, 1650−1655.
(32) Rubio-Marcos, F.; Romero, J. J.; Ochoa, D. A.; García, J. E.; Perez, R.; Fernández, J. F. Effects of Poling Process on KNN-Modified Piezoceramic Properties. *J. Am. Ceram. Soc.* **2010**, *93*, 318−321.
(33) http://www.ferroperm-piezo.com/files/files/Ferroperm%20Catalogue.pdf (accessed May 2003).
(34) Rubio-Marcos, F.; Marchet, P.; Merle-Méjean, T.; Fernández, J. F. Role of Sintering Time, Crystalline Phases and Symmetry in the Piezoelectric Properties of Lead-Free KNN-Modified Ceramics. *Mater. Chem. Phys.* **2010**, *123*, 91−97.
(35) Rubio-Marcos, F.; Romero, J. J.; Martín-Gonzalez, M. S.; Fernandez, J. F. Effect of Stoichiometry and Milling Processes in the Synthesis and the Piezoelectric Properties of Modified KNN Nanoparticles by Solid State Reaction. *J. Eur. Ceram. Soc.* **2010**, *30*, 2763−2771.
(36) Li, F.; Xiaon, D.; Wu, J.; Wang, Z.; Liu, C.; Zhu, J. Phase Structure and Electrical Properties of $(K_{0.5}Na_{0.5})NbO_3$−$(Bi_{0.5}Na_{0.5})$-ZrO_3 Lead-Free Ceramics with a Sintering Aid of ZnO. *Ceram. Int.* **2014**, *40*, 14601−14605.
(37) Chang, Y.; Yang, Z.; Xiong, L.; Liu, Z.; Wang, Z. Phase Structure, Microstructure, and Electrical Properties of Sb-Modified (K, Na, Li) (Nb, Ta) O_3 Piezoelectric Ceramics. *J. Am. Ceram. Soc.* **2008**, *91*, 2211−2216.
(38) Zhao, P.; Zhang, B.-P.; Tu, R.; Goto, T. High Piezoelectric d_{33} Coefficient in Li/Ta/Sb-Codoped Lead-Free (Na,K)NbO_3 Ceramics Sintered at Optimal Temperature. *J. Am. Ceram. Soc.* **2008**, *91*, 3078−3081.
(39) Zhang, B.; Wu, J.; Cheng, X.; Wang, X.; Xiao, D.; Zhu, J.; Wang, X.; Lou, X. Lead-free Piezoelectrics Based on Potassium−Sodium Niobate with Giant d_{33}. *ACS Appl. Mater. Interfaces* **2013**, *5*, 7718−7725.
(40) Ge, W.; Ren, Y.; Zhang, J.; Devreugd, C. P.; Li, J.; Viehland, D. A Monoclinic-Tetragonal Ferroelectric Phase Transition in Lead-Free $(K_{0.5}Na_{0.5})NbO_3$-x%$LiNbO_3$ Solid Solution. *J. Appl. Phys.* **2012**, *111*, 103503.
(41) Ramajo, L.; Castro, M.; del Campo, A.; Fernandez, J. F.; Rubio-Marcos, F. Influence of B-site Compositional Homogeneity on Properties of $(K_{0.44}Na_{0.52}Li_{0.04})$ $(Nb_{0.86}Ta_{0.10}Sb_{0.04})O_3$-Based Piezoelectric Ceramics. *J. Eur. Ceram. Soc.* **2014**, *34*, 2249−2257.
(42) Rubio-Marcos, F.; Marchet, P.; Romero, J. J.; Fernández, J. F. Structural, Microstructural and Electrical Properties Evolution of (K,Na,Li) (Nb,Ta,Sb)O_3 Lead-Free Piezoceramics through NiO Doping. *J. Eur. Ceram. Soc.* **2011**, *31*, 2309−2317.
(43) Li, E.; Kakemoto, H.; Wada, S.; Tsurumi, T. Influence of CuO on the Structure and Piezoelectric Properties of the Alkaline Niobate-Based Lead-Free Ceramics. *J. Am. Ceram. Soc.* **2007**, *90*, 1787−1791.
(44) Alkoy, E. M.; Papila, M. Microstructural Features and Electrical Properties of Copper Oxide added Potassium Sodium Niobate Ceramics. *Ceram. Int.* **2010**, *36*, 1921−1927.
(45) Zhang, B.; Wang, X.; Cheng, X.; Zhu, J.; Xiao, D.; Wu, J. Enhanced d_{33} Value in $(1-x)[(K_{0.50}Na_{0.50})0.97Li_{0.03}Nb_{0.97}Sb_{0.03}O_3]$−$xBaZrO_3$ Lead-Free Ceramics with an Orthorhombic−Rhombohedral Phase Boundary. *J. Alloys Compd.* **2013**, *581*, 446−451.
(46) Noheda, B.; Cox, D. E.; Shirane, G.; Gonzalo, J. A.; Cross, L. E.; Park, S.-E. A Monoclinic Ferroelectric Phase in the $Pb(Zr_{1-x}Ti_x)O_3$ Solid Solution. *Appl. Phys. Lett.* **1999**, *74*, 2059.
(47) Fu, H. X.; Cohen, R. E. Polarization Rotation Mechanism for Ultrahigh Electromechanical Response in Single-Crystal Piezoelectrics. *Nature* **2000**, *403*, 281−283.
(48) Noheda, B.; Cox, D. E.; Shirane, G.; Park, S.-E.; Cross, L. E.; Zhong, Z. Polarization Rotation Via a Monoclinic Phase in the Piezoelectric 92%$PbZn_{1/3}Nb_{2/3}O_3$-8%$PbTiO_3$. *Phys. Rev. Lett.* **2001**, *86*, 3891−3894.
(49) Kim, M. S.; Jeong, S. J.; Kim, I. S.; Song, J. S. Piezoelectric Properties of Li_2O Excess $(Na_{0.4875}K_{0.4625}Li_{0.05})$ $(Nb_{0.95}Ta_{0.5})O_3$ Ceramics by Conventional Sintering Method. *J. Ceram. Soc. Jpn.* **2009**, *117*, 592−595.
(50) Akdoğan, E. K.; Kerman, K.; Abazari, M.; Safari, A. Origin of High Piezoelectric Activity in Ferroelectric $(K_{0.44}Na0.52Li_{0.04})$−$(Nb_{0.84}Ta_{0.1}Sb_{0.06})O_3$ Ceramics. *Appl. Phys. Lett.* **2008**, *92*, 112908.
(51) Kakimoto, K.; Akao, K.; Guo, Y.; Ohsato, H. Raman Scattering Study of Piezoelectric $(Na_{0.5}K_{0.5})NbO_3$-$LiNbO_3$ Ceramics. *Jpn. J. Appl. Phys.* **2005**, *44*, 7064−7067.
(52) Rubio-Marcos, F.; Bañares, M. A.; Romero, J. J.; Fernández, J. F. Correlation between the Piezoelectric Properties and the Structure of Lead-Free KNN−Modified Ceramics, Studied by Raman Spectroscopy. *J. Raman Spectrosc.* **2011**, *42*, 639−643.
(53) Liu, G.; Zhang, S.; Jiang, W.; Cao, W. Losses in Ferroelectric Materials. *Mater. Sci. Eng., R* **2015**, *89*, 1−48.
(54) Ramajo, L.; Castro, M.; del Campo, A.; Fernandez, J. F.; Rubio-Marcos, F. Revealing the Role of Cationic Displacement in Potassium-Sodium Niobate Lead-Free Piezoceramics by Adding W^{6+} Ions. *J. Mater. Chem. C* **2015**, *3*, 4168−4178.

DOI: 10.1021/acsami.5b06747
ACS Appl. Mater. Interfaces 2015, 7, 23080−23088